ASEG-PESA 2015
Geophysics and Geology together for Discovery
24th International Geophysical Conference and Exhibition
15–18 February 2015 Perth, Western Australia

Variation of natural fracture orientations in the Carnarvon Basin's Rankin Platform and Dampier Sub-Basin, NWS, Western Australia

Adam H.E. Bailey
The University of Adelaide
North Terrace, Adelaide
adam.bailey@adelaide.edu.au

Rosalind C. King
The University of Adelaide
North Terrace, Adelaide
Rosalind.king@adelaide.edu.au

Simon P. Holford
The University of Adelaide
North Terrace, Adelaide
simon.holford@adelaide.edu.au

Joshua M. Sage
Beach Petroleum
Glenside, SA
joshua.sage@beachenergy.com.au

SUMMARY

Natural fractures in the Carnarvon Basin's Rankin Platform and Dampier Sub-Basin are identified using electrical resistivity image logs from 10 petroleum wells. In-situ stresses are diagnosed for the area using data from these and four additional wells, with these results indicating it likely that this study area hosts a relatively isotropic in-situ stress field.

Identified fractures occur at all orientations, and demonstrate no dominant trend. They do not reflect the in-situ stresses, nor the dominant north-northeast to northeast fault strikes. Rather, they most closely reflect the orientation of more local structures which the wells are adjacent to, demonstrating that natural fracture populations may be more dependent on local structure than dominant regional trends.

Key words: image logs, in-situ stress, natural fractures, Carnarvon Basin

INTRODUCTION

The Northern Carnarvon Basin is Australia's principle hydrocarbon producing basin (Barber, 2013), with the majority of current production from conventional oil and gas plays (Barber, 2013). Modern recovery methods can often be heavily reliant on secondary structural permeabilities provided by natural and enhanced fracture sets. In this study, we use resistivity based wellbore image logs from the Formation Micro-Imager (FMI) tool in order to identify detailed, high resolution, structural information on natural fractures present within 10 petroleum wells situated on the Rankin Platform at the margin of the Dampier Sub-Basin.

The Northern Carnarvon Basin's Dampier Sub-basin is one of a series of large en echelon rift depocentres containing a sedimentary succession dominated by Triassic, Jurassic, and Lower Cretaceous sediments (Tindale et al., 1998). It has a dominant north-northeast to northeast striking fault trend formed through oblique extension (Romine et al., 1997). Major extensional fault systems separate the Dampier Sub-basin from nearby structural highs such as the Rankin Platform (Stagg and Colwell, 1994), with broad marginal terraces such as the Enderby Terrace having formed over down-faulted and rotated blocks along the fault margins, including between the Rankin Platform and the Dampier Sub-basin (Kopsen and McGann, 1985). While the Carnarvon Basin hosts large inversion structures, these are primarily limited to the Exmouth Sub-basin, Exmouth Plateau, and Barrow Sub-Basin (Hocking 1990), with expression in the Dampier Sub-basin limited to transpressional reactivation of rift-related structures (Longley et al, 2002; Cathro and Karner, 2006). Present day, the Northern Carnarvon Basin has been demonstrated to likely host a strike-slip faulting stress regime (Neubauer et al, 2007) though there is neotectonic evidence for a reverse faulting regime (Hillis et al, 2008; Revets et al, 2009).

IN-SITU STRESSES FROM GEOPHYSICAL DATA

Data collected during petroleum exploration has proven valuable in constraining crustal stress orientations in continental regions (e.g. Bell, 1990). In-situ maximum horizontal stress (σ_H) orientations are derived from stress indicators such as borehole breakouts (BOs) and drilling induced tensile fractures (DITFs) in petroleum wells (Bell, 1996). Both BOs and DITFs form as a response to stress perturbations that exist around open wellbores (Kirsch 1898). Borehole breakouts are elongations of the borehole in the compressive regions of the borehole walls, and DITFs are vertical fractures formed in the tensile regions of the borehole wall (e.g. Brudy & Zoback 1999) (FIGURE 1). A total of 38 BOs and 5 DITFs were identified in the 10 image logs interpreted in this study, resulting in a regional mean σ_H orientation of 116°N for the study area.

In addition to the 10 wells featuring image logs, another four wells were used to help constrain stress magnitudes. Vertical stress magnitude (σ_V) is defined as the stress applied by the mass of overburden above a specific depth, and is calculated through an integration of rock densities to the depth of interest (Bell, 1996a). The calculated σ_V gradient in the study area varies from 20.4 MPa km-1 (bsb) to 22.7 MPa km-1 (bsb) in the Carnarvon Basin (TABLE 1) a variation of 2.3 MPa km-1.

Minimum horizontal stress magnitude (σ_h) can be deduced from fracture closure pressures and leak-off pressures obtained through hydraulic fracturing experiments, such as leak-off tests (LOT) (Bell, 1996). These involve sealing a section of wellbore during drilling and increasing hydraulic pressure until a fracture is formed (Bell, 1996). In this study, nine LOTs were used to constrain the magnitude of σ_h. Values of σ_h range from 12.66 MPa at 0.8 km to 50.3 MPa at 2.6 km (TABLE 1).

The magnitude of σ_H is estimated from relationships with σ_h (Bell, 1996). Rock strength can be assumed to be zero where tensile failure has occurred (Brudy & Zoback, 1999). Wells featuring DITFs and LOTs can therefore be used to estimate σ_H (Hubbert & Willis, 1957). Nine LOTs were used to estimate

σ_H magnitude, resulting in values that range from 16.6 MPa at 0.8 km to 71.0 MPa at 2.6 km (TABLE 1).

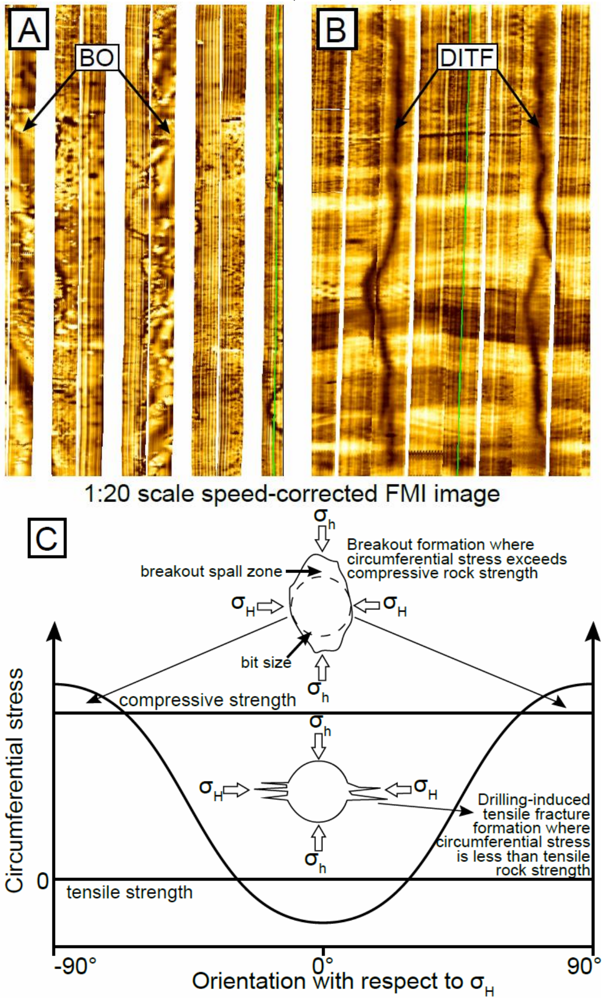

FIGURE 1: Sections of FMI image showing (A) borehole breakouts (BO) from Dixon-2 and (B) drilling-induced tensile fractures (DITFs); (C) azimuth of BO and DITFs with respect to the circumferential stress around the wellbore (Hillis & Reynolds, 2000).

NATURAL FRACTURES IN IMAGE LOGS

Natural fractures are common natural features that occur in the brittle crust, and which are often considered to be scale invariant (Walsh and Watterson, 1993; Nicol et al, 1995). As well as being present on all scales, natural fractures have been experimentally shown to enhance permeability within geologic media by up to several orders of magnitude (Brace, 1980). Significant permeability improvements are seen within rocks that feature low primary permeabilities and porosities, however, the effect is far more modest within permeable rocks (Nelson, 1977; Swolfs et al, 1981). Electrical resistivity image logs allow for simple identification of natural fractures, as they provide a high resolution pseudo-image of the borehole wall (FIGURE 2). Fractures appear on this image as sinusoids where the crest represents the up-dip part of the fracture and the trough represents the down-dip part of the fracture. The

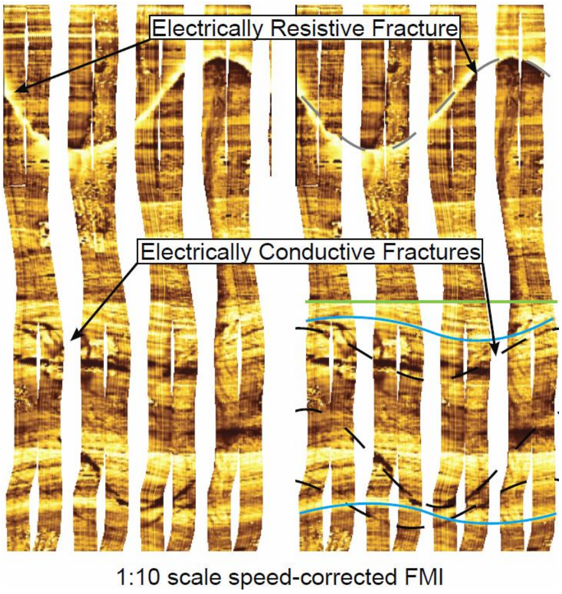

FIGURE 2: A section of FMI image showing electrically resistive (grey) and electrically conductive fractures (black). Examples of bedding are marked in blue and an erosional surface is marked in green, illustrating the similarity in appearance between syn-tectonic and non-tectonic features (Bailey et al., 2014).

amount of dip controls the amplitude of the sinusoid, with high amplitudes equal to steeply dipping fractures and low-amplitudes are equal to shallowly dipping fractures (FIGURE 2). Syn-tectonic features such as fractures can have very similar characteristics to non-tectonic features such as bedding and other sedimentary structures, and so it is important to distinguish between these (FIGURE 2). As all the wells utilised in this study are petroleum wells, they exhibit a clear sampling bias towards the Late Jurassic to Late Cretaceous sediments which contain proven reservoirs of natural gas.

A total of 500 fractures are identified in the 10 interpreted FMI logs (FIGURE 3), consisting of 177 electrically conductive and 323 electrically resistive fractures (FIGURE 3). It can be seen that there are no well-defined mean strike orientations, with fractures occurring at all orientations (FIGURE 3). A generally northeast-southwest trend is evident in the resistive fractures, accompanied by a northwest-southeast fracture trend and a general spread of fractures at all strikes (FIGURE 3).

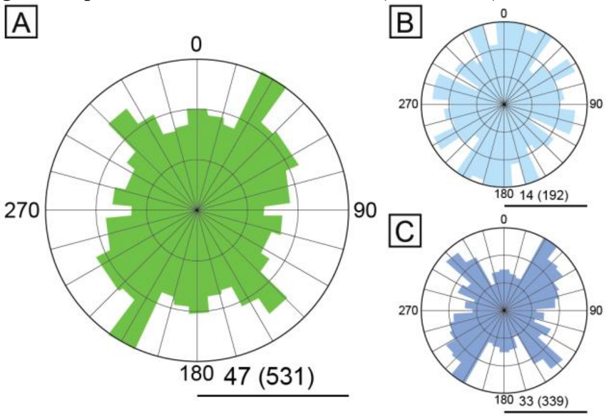

FIGURE 3: Rose diagrams showing strike orientation of fractures identified in image logs for (A) all fractures; (B) conductive fractures; (C) resistive fractures.

DISCUSSION AND CONCLUSIONS

The study area can be seen to host an array of fracture orientations which appear to occur without a systematic orientation, and which are seemingly unrelated to the dominant structural trends or in-situ stress. However, when this regional presentation of data is decomposed into the component wells and compared to the local structure (10 kms), it is observed that fracture orientations reflect the structures adjacent to the wells (FIGURE 4). Additionally, there is likely to be a secondary control on fracture orientation for these wells, as in-situ stress magnitudes along the western margin of the Dampier Sub-Basin and through the Rankin Platform are thought to be close to isotropic; with σ_H and σ_V approximately equal and possibly interchangeable, and σ_h close in magnitude to σ_H and σ_V (TABLE 1). This is compared the rest of the Carnarvon Basin where distinctly anisotropic stress magnitudes are calculated (Neubauer et al., 2007). As a result, where there is no structure dictating fracture orientations, there is no overriding stress orientation controlling fracture propagation orientation. Fractures may therefore form as the stress field fluctuates into anisotropy due to local perturbations (e.g. fluid pressure), which under the regime could result in any of the principle stresses becoming the maximum, and, therefore, fractures forming at any orientation (Tewksbury et al., 2014). Hence, the scattering in fracture observations observed as a secondary trend within the Dampier Sub-Basin wells. The possibility of there being lithological or rock property controls over fracture formation in this region was also discounted, with an analysis of fracture occurrence compared to calculated and measured rock properties including lithological logs, unconfined compressive strength, Poisson's Ratio, and Young's Modulus, so a structural and stress based cause is the most likely and is supported by our data.

ACKNOWLEDGMENTS

The authors would like to thank the South Australian Centre for Geothermal Energy Research and The Australian Society of Exploration Geophysicists Research Foundation (RF12P01) for their generous support in this project. Special thanks go to the Western Australian Department of Mines and Petroleum for their assistance in much of the data we have used.

REFERENCES

Bailey, A., R. King, S. Holford, J. Sage, G. Backe, and M. Hand. 2014. Remote sensing of subsurface fractures in the Otway Basin, South Australia, J. Geophys. Res. Solid Earth, 119, doi:10.1002/2013JB010843

Barber, P.M. 2013, Oil Exploration Potential in the Greater Northern Australian - New Guinea Super Gas Province, in Keep, M. & Moss, S.J. (Eds), 2013, The Sedimentary Basins of Western Australia IV: Proceedings of the Petroleum Exploration Society of Australia Symposium, Perth, WA, 2013

Bell, J.S. 1990. Investigating stress regimes in sedimentary basins using information from oil industry wireline logs and drilling records. In: Hurst, A., Lovell, M.A. (eds.) Geological Applications of Wireline Logs. Geological Society of London, Special Publication, 48, 305–325.

Bell, J.S. 1996. In situ stresses in sedimentary basins (part 1): measurement techniques. Geoscience Canada 23, 85–100.

Brace, W. 1980, Permeability of crystalline and argillaceous rocks, paper presented at International Journal of Rock Mechanics and Mining Sciences & Geomechanics Abstracts, Elsevier.

Brudy, M. & Zoback, M.D. 1999, Drilling-induced tensile wall-fractures: implications for determination of in-situ stress orientation and magnitude. International Journal of Rock Mechanics and Mining Sciences, 36 (2), 191-215.

Cathro, D.L. and Karner, G.D., 2006. Cretaceous–Tertiary inversion history of the Dampier Sub-basin, northwest Australia: insights from quantitative basin modelling. Marine and Petroleum Geology, 23, 503–526.

Hillis, R.R. & Reynolds, S.D. 2000. The Australian Stress Map. Journal of the Geological Society, London, 157, 915-921. doi:10.1144/jgs.157.5.915

Hillis, R.R., Sandiford, M., Reynolds, S.D., & Quigley, M.C. 2008. Present-day stresses, seismicity and Neogene-to-Recent tectonics of Australia's 'passive' margins: intraplate deformation controlled by plate boundary forces. In: Johnson, H., Doré, T.G., Gatliff, R.W., Holdsworth, R.W., Lundin, E.R., & Ritchie, J.D. (eds.) The Nature and Origin of Compression in Passive Margins. Geological Society of London, Special Publication, 306, 71–90.

Hocking, R.M., 1990. Carnarvon Basin. In: Geology and Mineral Resources of Western Australia. Western Australia Geological Survey, Memoir 3, 457–495.

Kirsch, V. 1898. Die Theorie der Elastizität und die Bedürfnisse der Festigkeitslehre. Zeitschrift des Vereines Deutscher Ingenieure, 29, 797-807.

Kopsen, E. and Mcgann, G., 1985. A review of the hydrocarbon habitat of the eastern and central Barrow-Dampier Sub-basin, Western Australia. The APEA Journal, 25(1), 154–176.

Longley, I.M., Buessenschuett, C., Clydsdale, L., Cubitt, C.J., Davis, R.C., Johnson, M.K., Marshall, N.M., Murray, A.P., Somerville, R., Spry, T.B. and Thompson, N.B., 2002. The North West Shelf of Australia – a Woodside perspective. In: Keep, M. and Moss, S.J. (eds), The Sedimentary Basins of Western Australia 3: Proceedings of the Petroleum Exploration Society of Australia Symposium, Perth, 27–88.

Neubauer, M.C., Hillis, R.R., King, R.C., & Reynolds, S.D. 2007. The contemporary stress field of the offshore Carnarvon Basin, North West Shelf, Western Australia. In: Eberhardt, E., Stead, D. & Morrison, T. (eds.) Rock Mechanics: Meeting Society's Challenges and Demands: Proceedings of the 1st Canada-U.S. Rock Mechanics Symposium, 27-31 May 2007, Taylor & Francis, ISBN: 0415444012

Nelson, R. A., and J. Handin (1977), Experimental study of fracture permeability in porous rock, AAPG Bulletin, 61(2), 227-236.

Nicol, A., J. J. Walsh, J. Watterson, and P. G. Bretan (1995), Three-dimensional geometry and growth of conjugate normal faults, Journal of Structural Geology, 17(6), 847-862

Revets, S.A., Keep, M., & Kennett, B.L.N. 2009. NW Australian intraplate seismicity and stress regime. Journal of Geophysical Research, 114, B10305, doi:10.1029/2008JB006152

Romine, K.K., Durrant, J.M., Cathro, D.L., & Bernardel, G. 1997. Petroleum play prediction for the Cretaceous-Tertiary basin phase, Northern Carnarvon Basin. Australian Petroleum Production and Exploration Association Journal, 37, 315–339.

Stagg, H.M.J. and Colwell, J.B., 1994. The structural foundations of the Northern Carnarvon Basin. In: Purcell, P.G. and Purcell, R.R. (eds), The Sedimentary Basins of Western Australia: Proceedings of the Petroleum Exploration Society of Australia Symposium, Perth, 1994, 349–364.

Swolfs, H., C. Brechtel, W. Brace, and H. Pratt (1979), Mechanical properties of a jointed sandstone, Geophysical Monograph Series: Mechanical Behavious of Crustal Rocks, 24, 161-172.

Tewksbury, B.J., Hogan, J.P., Kattenhorn, S.A., Mehrtens, C.J., and Tarabees, E.A., 2014, Polygonal faults in chalk: Insights from extensive exposures of the Khoman Formation, Western Desert, Egypt: Geology, 42, 479–482.

Tindale, K., Newell, N., Keall, J., & Smith, N. 1998. Structural evolution and charge history of the Exmouth Sub-Basin, Northern Carnarvon Basin, Western Australia. In: Purcell, P.G. & Purcell, R.R. (Eds.), Western Australian Basins Symposium II. Petroleum Exploration Society of Australia (PESA), 447–472.

Walsh, J. J., and J. Watterson 1993, Fractal analysis of fracture patterns using the standard box-counting technique: valid and invalid methodologies, Journal of Structural Geology, 15(12), 1509-1512.

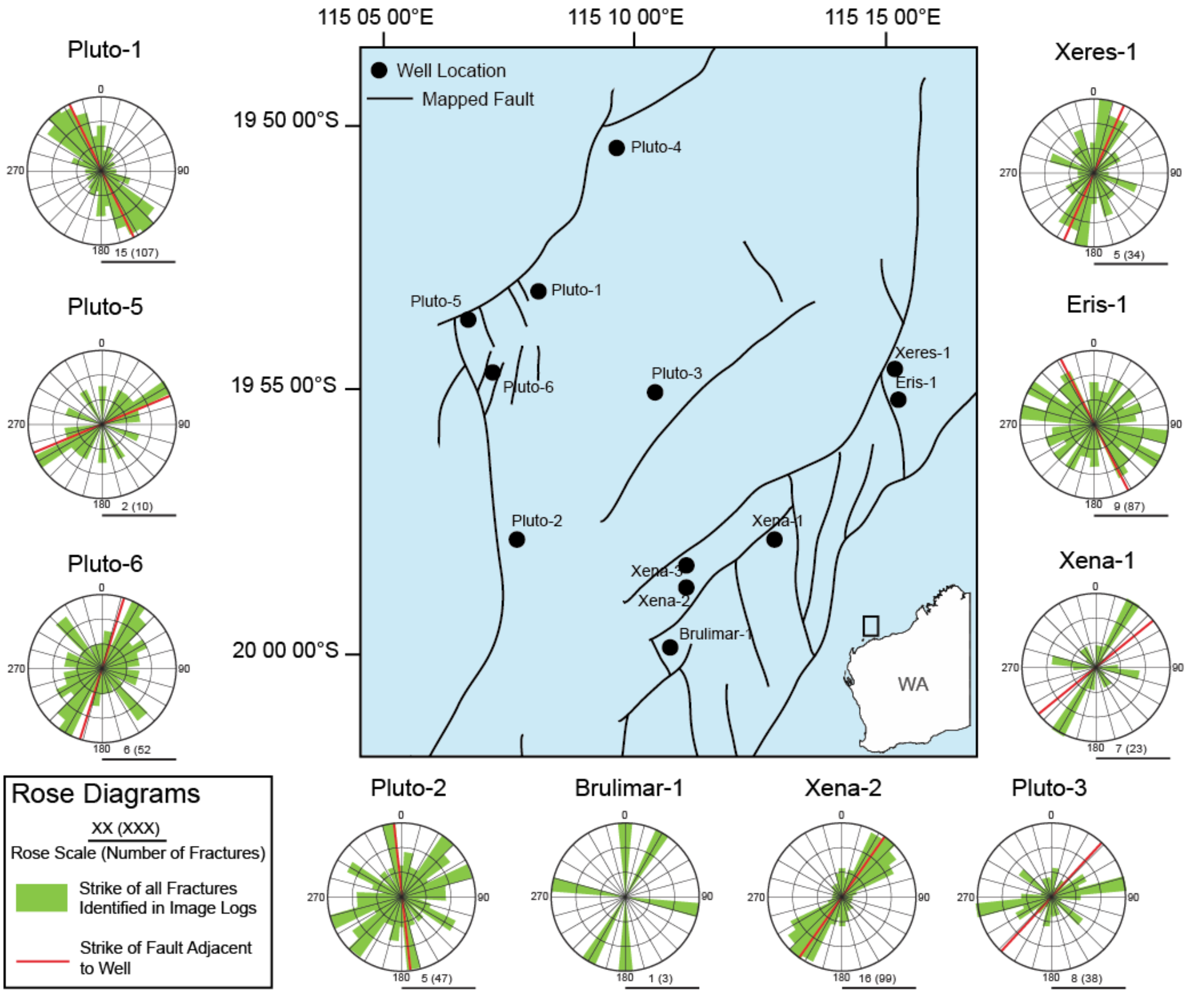

Figure 4: Map of locations of wells featuring interpreted FMI logs, and the proximity of those wells to local structural features. Rose diagrams are for fracture orientations from each well, compared to the strike (red line) of the fault adjacent to that well. Well Brulimar-1 lacks a line due to the low number of identified fractures.

Well	FMI Interval (m)	LOT Depth (m)	σ_h (MPa)	σ_V (Mpa/km)	σ_H (MPa)
Brulimar-1	3023 - 3271	1338.6	22.8	-	-
Dixon-2	-	1849.9	30.15	-	-
Eris-1	2149 - 3258	-	-	-	-
Lady Nora-1	-	1940.07	33.04	-	44.28
Pluto-1	2141 - 3275	-	-	20.4	-
Pluto-3	2215 - 3528	-	-	21.4	-
Pluto-4	-	1259	20.4	-	26.7
Pluto-5	2738 - 3165	1085.16	22.07	21.1	-
Pluto-6	2345 - 3285	-	-	21	-
Wheatstone-2	-	774.8	12.66	-	16.6
Wheatstone-2	-	2639.8	50.34	-	71
Xena-1	-	2116	36.6	21.5	-
Xena-2	2235 - 3568	-	-	22.4	-
Xena-3	2315 - 3517	2094.8	35.4	22.7	-
Xeres-1	2291 - 3217	-	-	21.8	-

Table 1: Depths (m) of image log intervals, leak-off tests (LOTs) and estimated values for the three principle stresses for the wells used in this study.